

Supporting information for

Multiformity and fluctuation of Cu ordering in Cu₂Se thermoelectric materials

Ping Lu^{a,b,c}, Huili Liu^{a,c}, Xun Yuan^{a,c}, Fangfang Xu^{*,a,b}, Xun
Shi^{*,a}, Kunpeng Zhao^{a,c}, Wujie Qiu^a, Wenqing Zhang^a,
Lidong Chen^a

^a State Key Laboratory of High Performance Ceramics and Superfine Microstructures, and

^b Analysis and Testing Center for Inorganic Materials, Shanghai Institute of Ceramics, Chinese Academy of Sciences (CAS), 1295 Dingxi Road, Shanghai 200050, China

^c University of Chinese Academy of Sciences, 19 Yuquan Road, Beijing 100049, China

The detailed information of S3 structure predicted by the first-principle calculation is list in Table S1.

Table S1. Lattice parameters of the predicted S3 structure (space group: P1) with $a=7.545\text{\AA}$,
 $b=12.416\text{\AA}$, $c=7.110\text{\AA}$, $\alpha=90.030^\circ$, $\beta=108.395^\circ$, and $\gamma=90.342^\circ$.

Atom	x/a	y/b	z/c	Atom	x/a	y/b	z/c
Cu1	0.65872	0.16449	0.54796	Cu19	0.31222	0.98502	0.94233
Cu2	0.68551	0.48925	0.56271	Cu20	0.32016	0.32877	0.93937
Cu3	0.74949	0.82805	0.58204	Cu21	0.18823	0.65965	0.89654
Cu4	0.44097	0.14872	0.17336	Cu22	0.55579	0.96902	0.3474
Cu5	0.43053	0.53431	0.12898	Cu23	0.56427	0.34267	0.2819
Cu6	0.42916	0.79832	0.11399	Cu24	0.54841	0.67065	0.41159
Cu7	0.6878	0.01493	0.05711	Se25	0.23425	0.15781	0.75488
Cu8	0.81196	0.34026	0.103	Se26	0.22717	0.4928	0.7405
Cu9	0.67972	0.67116	0.06024	Se27	0.21603	0.82655	0.7325
Cu10	0.44426	0.03092	0.65213	Se28	0.22307	0.0022	0.24493
Cu11	0.45155	0.32949	0.58806	Se29	0.22036	0.34161	0.24348
Cu12	0.43576	0.65726	0.71762	Se30	0.2116	0.67318	0.24038
Cu13	0.2508	0.17202	0.41755	Se31	0.78395	0.17341	0.26705
Cu14	0.31423	0.51083	0.43682	Se32	0.77281	0.50712	0.25903

Cu15	0.34115	0.8356	0.4516	Se33	0.76575	0.84215	0.2446
Cu16	0.57077	0.20171	0.88553	Se34	0.777	0.99786	0.75458
Cu17	0.56946	0.46568	0.87096	Se35	0.78836	0.32688	0.75909
Cu18	0.55912	0.85119	0.8261	Se36	0.77959	0.65846	0.75607

Table S2. Energies of different structures calculated by the first-principles method. The energy of the cubic β -phase (S0) is set as reference and energies are rescaled for one Cu_2Se formula unit.

Structure Label	Space Group	E(eV)
S0	$Fm\bar{3}m$ (225)	0
S1	$P\bar{1}$ (2)	-0.2921
S2	$C2/c$ (15)	-0.2920
S3	$P1$ (2)	-0.2990

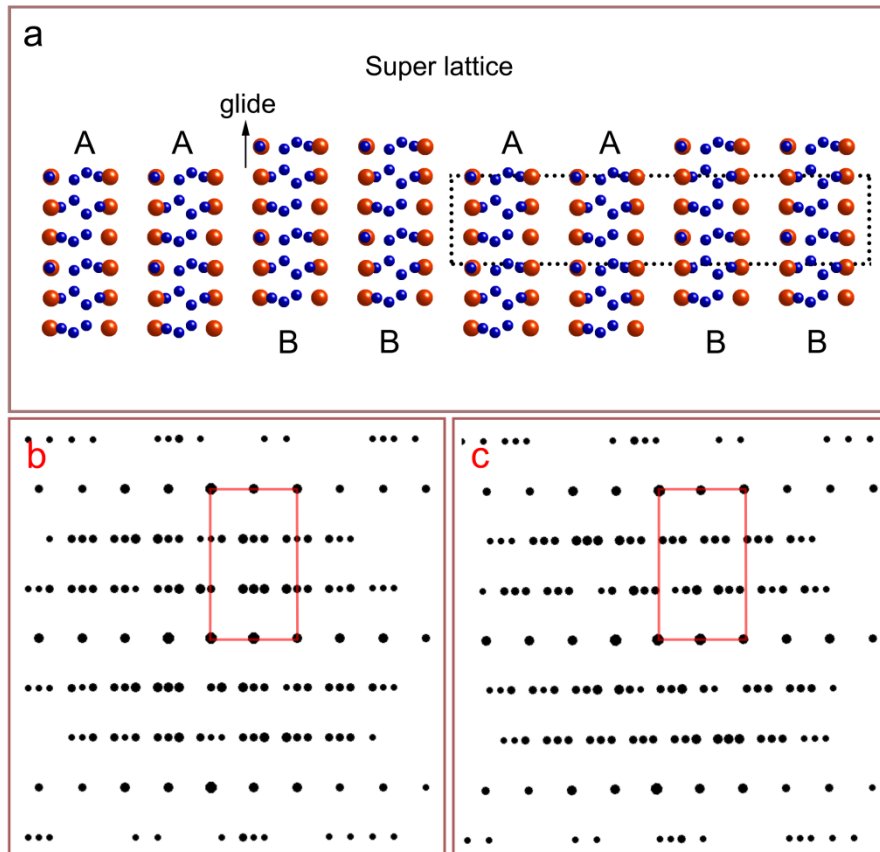


Figure S1. A possible structure for the four-fold periodic packing sequence: (a) is the structure model consisting of four S1-type layers and a $1/6\langle 211 \rangle_c$ -type displacement is involved in-between every two layers. (b) and (c) are the simulated electron diffraction patterns according to the structural model projected along two different $\langle 112 \rangle_c$ directions. They match the experimental observations in Fig. 2e and Fig. 2f, respectively in the manuscript.

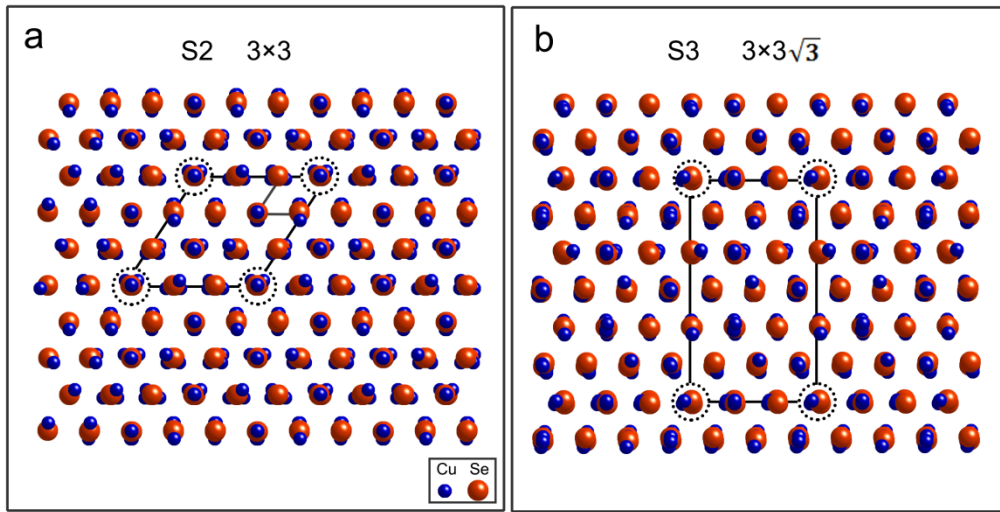


Figure S2. The structural models projected perpendicular to the layer plane: (a) is for S2, which shows a 3×3 super cell compared to the *fcc* cell. (b) is for S3, which shows a $3 \times 3\sqrt{3}$ super cell.

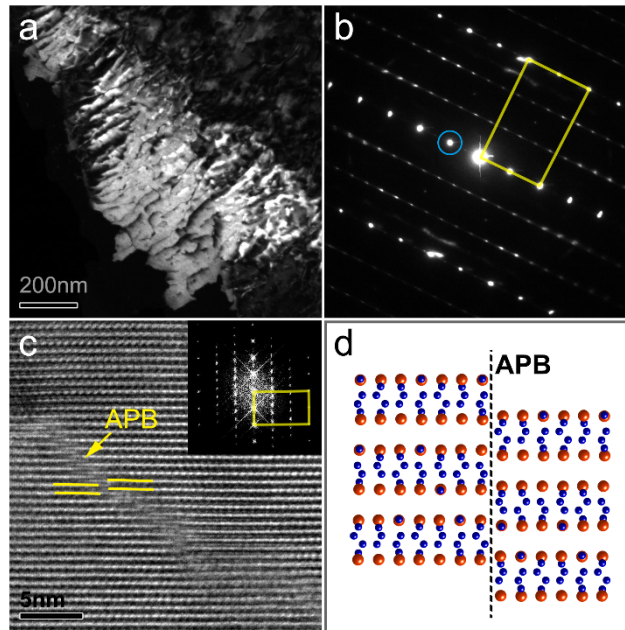


Figure S3. Domain structures in the Cu_2Se ingot: (a) is the dark-field image using the cycled reflection (i.e. $1/2\{111\}_c$) in the diffraction pattern (b). (c) is the HREM image showing an antiphase boundary (APB) indicated by an arrow. (d) is the structure model of the APB.

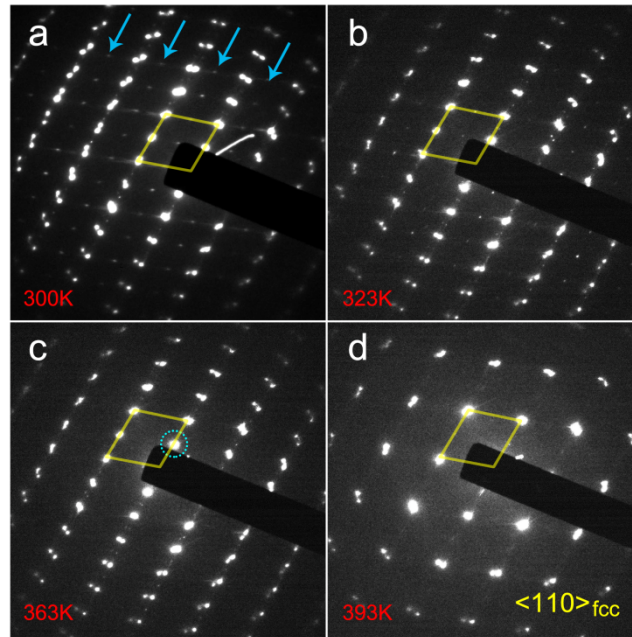


Figure S4. Evolution of the electron diffraction pattern at elevating temperatures: The diffraction patterns of the powder sample at room temperature, 323K, 363K, and 393K are shown in (a), (b), (c), and (d), respectively. Extra arrays of reflections (marked by arrows) are peculiar to S3 and they disappear at 363K, a temperature before the phase transition owing to the lower energy of S3. The spots cycled in green on (c) are related to the lamellar structure, which disappear at 393K (where phase transition takes place) eventually giving a typical $\langle 110 \rangle$ -projected pattern of the face-centered cubic.

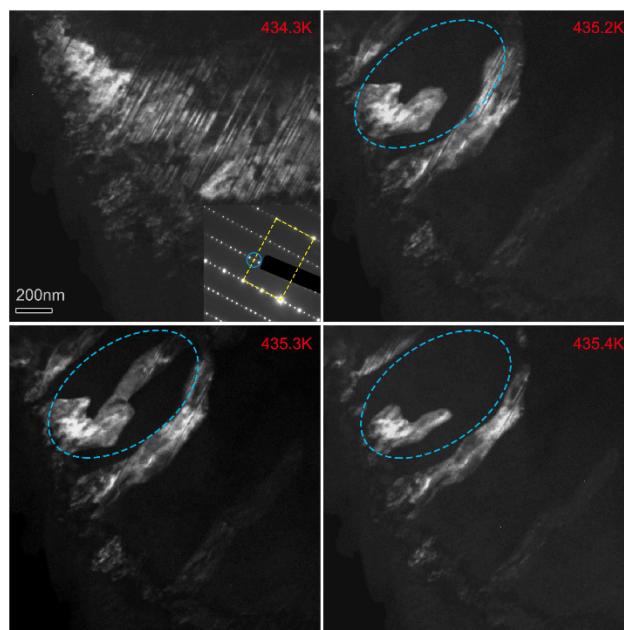


Figure S5: Evolution of dark-field images upon heating showing oscillation of order-disorder transition in local area. The dark-field images were acquired using circled reflections shown in the inset.

Table S3. Room temperature heat capacity and sound velocity of some typical thermoelectric materials.

Compounds	Heat capacity ($\text{J g}^{-1} \text{K}^{-1}$)	Sound velocity (m s^{-1})	Reference
AgSbTe ₂	0.205	4800	33
CoSb ₃	0.235	2934	34
Bi ₂ Te ₃	0.156	1601	40
PbTe	0.149	1830	41
In ₄ Se ₃	0.251	---	38
Zn ₄ Sb ₃	0.294	2470	35
Ba ₈ Ga ₁₆ Ge ₃₀	0.307	3046	36
Cu ₂ Se	0.363	2523	13